Nano-single crystal coalesced PtCu nanospheres as robust bifunctional catalyst for hydrogen evolution and oxygen reduction reactions

Wenqiang Li [a,b], Zhi-Yi Hu [a,c], Zhiwei Zhang [a], Ping Wei [c,d], Jianan Zhang [e,*], Zonghua Pu [a], Jiawei Zhu [a], Daping He [a], Shichun Mu [a,*], Gustaaf Van Tendeloo [a,f]

[a] State Key Laboratory of Advanced Technology for Materials Synthesis and Processing, Wuhan University of Technology, Wuhan 430070, China
[b] Henan Key Laboratory of Function-Oriented Porous Materials, College of Chemistry and Chemical Engineering, Luoyang Normal University, Luoyang 471934, China
[c] NRC (Nanostructure Research Centre), Wuhan University of Technology, Wuhan 430070, China
[d] International School of Materials Science and Engineering, Wuhan University of Technology, Wuhan 430070, China
[e] College of Materials Science and Engineering, Zhengzhou University, Zhengzhou 450001, China
[f] EMAT (Electron Microscopy for Materials Science), University of Antwerp, Groenenborgerlaan 171, Antwerp B-2020, Belgium

ARTICLE INFO

ABSTRACT

Because of high electrocatalytic activity, Pt based metal nanospheres (NSs) have attracted a lot of attention. Hence, multi-particle nano-single crystal coalesced PtCu NSs are designed and successfully synthesized by a cost-effective aqueous solution method. The formed PtCu NS catalyst exhibits a superior hydrogen evolution reaction (HER) electrocatalytic activity with an ultralow onset potential of 18 mV at the current density of 2 mA/cm^2 and high mass activity of 1.08 A/mg$_{Pt}$ (7.2 times higher than that of commercial Pt/C catalysts). Also, it shows an enhancement of 3.2 and 2.7 times in the mass and specific activities toward oxygen reduction reaction (ORR) compared to that of Pt/C. Moreover, it possesses an excellent catalytic durability for both ORR and HER. Even after 10,000 cycles, its ORR mass activity retains 87% of its initial value. The density functional theory (DFT) calculations demonstrate that by introducing Cu atoms into the Pt lattice, a downshift of the D-band center and favorable hydrogen adsorption free energy of approaching to zero (ΔG) occur, indicating the increased electrocatalytic activity of Pt electrocatalysts.

1. Introduction

Water splitting and fuel cells are two important energy conversion ways with high-efficiency and environmentally friendliness. Among them, hydrogen evolution reaction (HER) and oxygen reduction reaction (ORR) can influence their work efficiency [1,2]. It is well-known that the noble metal Pt is the best HER and ORR catalysts. However, the high cost, extreme scarcity and poor durability of Pt seriously limit its widespread applications [3–5]. Thus, to maximize the utilization of Pt for energy conversion, it is an important task to develop novel Pt-based catalysts with both superior activity and durability [6–8].

To date, for improving the catalytic performance, many approaches have been developed to prepare different nanostructure Pt-based catalysts. Among them, introducing transition metal atoms into the Pt lattice is a common strategy to elevate the utilization efficiency of Pt by improving the mass activity toward both

ORR and HER. When the transition metal atoms (M = Co, Ni, Fe, or Cu) are embedded into the Pt to form alloys, the compressive strain and electronic ligand effects imparted can increase [9,10]. When a certain threshold is reached, the surface activity toward the electrochemical reduction of O$_2$ will be enhanced in comparison with polycrystalline Pt [11–14]. For instance, PtNi and PtCo alloys exhibit superior electrocatalytic activity and high current densities [15,16]. Cu as a cheap transition metal can be easily introduced into Pt to form a Pt-Cu compound. In addition, Pt-Cu alloys are prominent electrochemical catalysts with a reduced sensitivity toward CO [17,18].

Another solution to increase the utilization efficiency of Pt is to prolong the lifespan of Pt-based catalysts. Up to now, most Pt-M nanocatalysts are based on zero-dimensional (0D) nanocrystals. However, the catalyst based on the 0D nanoparticle (NP) morphology readily agglomerate under high current densities or long-term tests during HER/ORR processes, resulting in poor stability [19]. However, compared to the commercial Pt, Pt nanocubes, nanowires and nanotubes have longer durability [20–24]. In particular, compared to separated Pt, the durability of the three-dimensional

(3D) structure comprised of interconnected metallic particles or filaments, can be improved. Therefore, rational design and facile synthesis of 3D Pt-based nanostructure catalysts are critical for maximizing the Pt utilization and stability [3,25,26].

Subsequently, we present a novel method to synthesize the 3D Pt-Cu nanospheres (PtCu NSs) by using the CoCuO nanowires (NWs) as seed, and further investigate the HER performance in a 0.5 M H_2SO_4 solution and the ORR performance in a 0.1 M $HClO_4$ solution. The novel PtCu NSs show significantly higher catalytic activity and durability than that of the commercial Pt/C catalyst for both ORR and HER. Finally, the activity enhancement mechanism of PtCu NSs is elaborated by density functional theory (DFT) calculations.

2. Experimental section

2.1. Preparation of PtCu NSs

8 mg CuCoO NWs were dissolved in the 20 ml ethylene glycol to form uniform solutions. The mixture solution was transferred into the 3 mouth flask. Then, 1 g AA (Ascorbic acid) and 17 ml H_2PtCl_6·$6H_2O$ solutions were added into the solutions. The mixture solution was stirred for 5 h at 50 °C. After cooled down to room temperature, the black product was collected and washed with ethanol and DI water several times before drying at 60 °C for overnight. The detailed preparation process of CoCuO NWs and PtCu NPs/C are seen in Supplementary Material.

2.2. Preparation of PtCu NSs/C

5 mg PtCu nanospheres and 10 mg XC-72 carbon were dispersed in a certain amount of ethanol, mixed and ultrasound for around 2 h to prepare PtCu NSs/C. The sample was collected by centrifugation and washed with ethanol for several times. At last, the product was dried under the vacuum condition. The related material characterization and computational details are present in Supplementary Material.

2.3. Electrochemical measurements

Electrochemical measurements were carried out with a three-electrode system on an electrochemical workstation (CHI 660E). The working electrode was a rotating disk electrode (RDE) (diameter: 5 mm, area: 0.196 cm^2).The platinum wire or graphite road was used as the counter electrode for ORR or HER, and the saturated calomel electrode (SCE) was used as the reference electrode. The catalyst ink was prepared by ultrasonically mixing a certain amount of catalyst with 900ul isopropyl alcohol, 100ul water and 20 ul 5 wt% Nafion solutions for 30 min. Then the suspension was deposited on a glassy carbon electrode. The Pt loading of PtCu NSs/C, PtCu NPs/C and Pt/C(JM) were 18.9 μg/cm^2, and 20.4 μg/cm^2, 20.9 μg/cm^2, respectively. The absolute amount of catalysts and Pt are shown in the Supplementary Material.

The catalysts were first subject to cyclic voltammetry (CV) scans between 0 and 1.2 V at 100 mV/s in N_2-saturated 0.1 M $HClO_4$ until a stable CV obtained (typically 200 cycles) before measuring the oxygen reduction reaction (ORR). ORR measurements were conducted in a 0.1 M $HClO_4$ solution filled with oxygen during the measurement. The sweep rate for ORR measurement was 50 mV/s. The ORR polarization curves were recorded by LSV at the scan rate of 10 mV/s in a O_2-saturated 0.1 M $HClO_4$ solution with the GC-RDE rotating at 1600 rpm. The accelerated durability tests (ADTs) of catalysis were performed in a O_2-staturated 0.1 M $HClO_4$ solution by applying cyclic potential sweeps between 0.6 and 1.0 V at 100 mV/s for 10,000 cycles. Both the calculation equations for

electrochemically active surface area (ECSA) and the mass activity of Pt are present in the Supplementary Material.

HER polarization curves were recorded by LSV at a sweep rate of 5 mV/s in 0.5 M H_2SO_4 solution. The durability of catalysts for HER was conducted by cycling the potential between −0.1 and 0.2 V at 100 mV/s for 5000 cycles. All polarization curves were iR-compensated. The iR-compensated potential was obtained after the correction of solution resistance measured following the equation: $E_{corr} = E−iR$, where E is the original potential, R is the solution resistance (7.9 Ω in 0.5 M H_2SO_4), i is the corresponding current, and E corr is the iR-compensated potential. The detailed iR-compensated process is shown in the Supplementary Material. The double layer capacitance (Cdl) was measured by cyclic voltammetry curves with sweep rates of 20, 40, 60, 80, 100 and 120 mV/s.

3. Results and discussion

3.1. Electrocatalyst characterizations

As shown in Fig. 1A, PtCu NSs can be synthesized in two steps: first, CoCuO nanowires (NWs) form hydrothermally in the presence of Co, Cu precursors and urea. Second, the mixing solution of CoCuO NWs, ascorbic acid and H_2PtCl_6·$6H_2O$ is vigorously stirred for 5 h at 50 °C to generate PtCu NSs. The mechanism of the transformation from 1D NWs to 3D NSs can be described as follows: at the beginning of the reaction, chloroplatinic acid reacts with the as prepared CoCuO NWs to form Co^{2+} and Cu^{2+} ions. It is well-known that the redox potential of Cu^{2+} and $PtCl_4^{2-}$ ($PtCl_6^{2-}$ + 2e → $PtCl_4^{2-}$+2-Cl^-) is + 0.342 V and + 0.758 V, respectively, which is much higher than that of Co^{2+} (-0.28 V). For this reason, Cu^{2+} and Pt^{2+} are more reductive than Co^{2+}. So Cu^{2+} and Pt^{2+} ions can be reduced by ascorbic acid (AA) at 50 °C and cohere to form PtCu alloy NSs, while the Co^{2-} ions cannot be reduced in the same synthesis process, and then are removed after washing. Here, it is worth noting that CuCoO nanowires play a double role during the reaction. First, it supplies the Cu source for the PtCu alloy. Second, based on the colour change as shown in Fig. S1, the Cu ions in $Cu(NO_3)_2$ cannot be reduced at 50 °C. Thus, it slowly controls the kinetics of Cu ion reduction in 5 h reaction time. Hence, we chose CuCoO nanowires as the Cu source.

X-ray diffraction (XRD) patterns of Pt/C, PtCu NSs and PtCu NPs are present in Fig. 1B and Fig. S2. By comparison with the standard Pt pattern, the peaks located at 39.8°, 46.3 °C, 67.7°, 81.6° can be assigned to the (1 1 1), (2 0 0), (2 2 0) and (3 1 1) planes of Pt, respectively. In the case of PtCu NSs, the Pt (1 1 1) diffraction peak appears at 40.2° with a positive shift compared with Pt/C (39.8°); no peaks are related to pure Cu or its oxides in Fig. 1B, indicating a contraction of the lattice by incorporation of Cu atoms into the fcc structure of Pt due to the formation of alloys [27]. It also proves that the as prepared sample is PtCu alloy, not a mixture of Pt and PtCu alloy.

X-ray photoelectron spectroscopy (XPS) was used to examine the composition and valence state of the alloyed PtCu NSs/C. As presented in Fig. 1C and Fig. S3, the peaks at 71.49 eV, 284.7 eV, 533.02 eV and 932.5 eV are attributed to the Pt 4f, C1s, O1s and Cu 2p signal, respectively, demonstrating the presence of Pt, Cu, C and O atoms. According to the XPS data, the atom ratio of Pt to Cu on the surface of PtCu NSs is about 76:24. But from inductively coupled plasma optical emission spectrometry (ICP) measurements over a large area, it reveals an atomic ratio of Pt and Cu 69:31. This indicates that the alloyed PtCu NSs have a Pt-rich outer surface [18]. Among them, the C and O elements could predominantly come from the XC-72 carbon as the support. The chemical state of Pt in PtCu NSs is shown in Fig. 1D. The asymmetric Pt 4f core shell (CL) spectrum can be deconvoluted into two pairs of
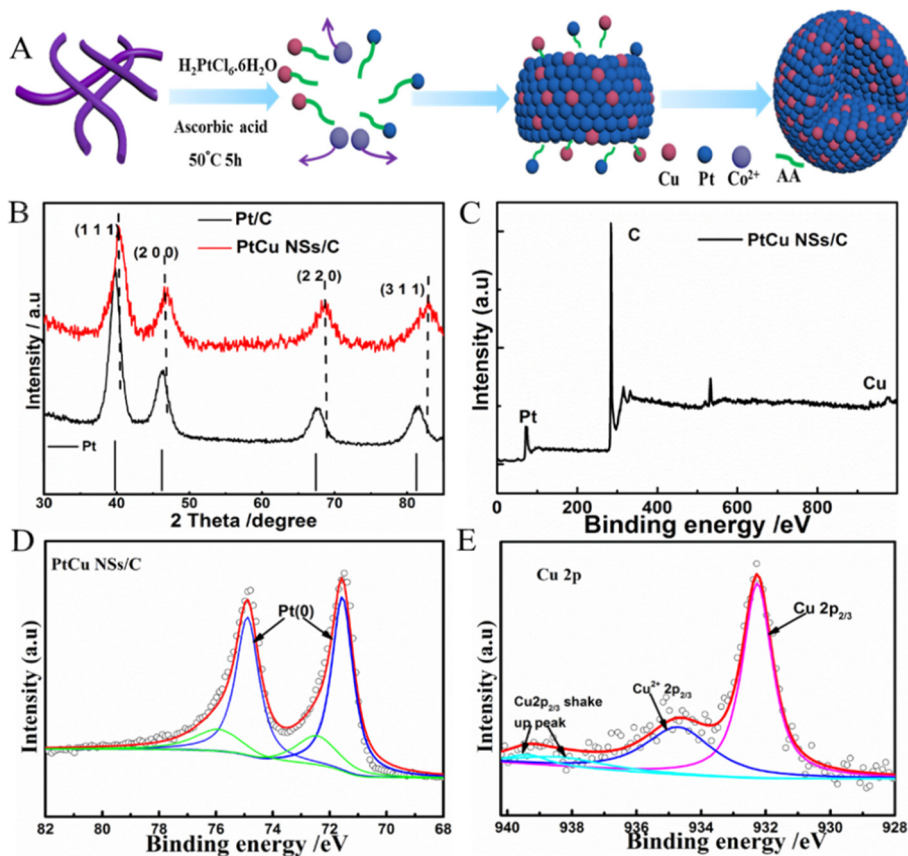
Fig. 1. (A) Schematic presentation of the formation process of PtCu nanospheres (NSs). (B) X-ray diffraction patterns of Pt/C, PtCu NSs/C. (C) XPS survey-scan of spectrum of PtCu NSs/C. (D) XPS spectrum of Pt 4f and (E) Cu 2p for PtCu NSs/C.

doublets due to the presence of Pt (0) and Pt (II). The Cu 2p spectrum (Fig. 1E) exhibits that although most of Cu atoms are in the form of metallic Cu (0) (932.3 eV), a weak signal from Cu (II) (934.78 eV) is also detected. A Pt 4f spectrum of Pt/C and PtCu NPs is further presented in Fig. S4. It is clearly seen that the Pt 4f7/2 peaks (Pt0) of the PtCu NS catalysts shift to a lower binding energy compared to that of the Pt/C and PtCu NP catalysts. After alloyed with Cu atoms, the negative shift of the Pt 4f CL binding energy in PtCu NSs (Table S1) indicates a downshift of the d-band center, leading to a decreased electron back-donation from the Pt 5d orbital and consequently accelerated ORR [28–31].

Fig. S5 shows a scanning electron microscopy (SEM) image of CuCoO NWs. The SEM image of as synthesized PtCu NSs in Fig. S6 confirms the spherical morphology. To further explore the detailed structure of PtCu NSs, transmission electron microscope (TEM) and high resolution transmission electron microscope (HRTEM) observations were performed. The low magnification high angle annular dark field scanning transmission electron microscopy (HAADF-STEM) image of Fig. 2A shows some PtCu NSs with a diameter of 40–100 nm, and the corresponding selected area electron diffraction (SAED) pattern (Fig. 2B) exhibits high degree of crystallinity and can be indexed based on a fcc lattice. Fig. 2C displays a rough surface of NSs. The high resolution HAADF-STEM image (Fig. 2D) and the corresponding FFT pattern (Fig. 2D inset) demonstrate that PtCu NSs consist of a large number of single crystal NPs. Namely, the PtCu NSs are assembled with small NPs which are connected each other to form a network. The EDX elemental maps (Fig. 2E–G) exhibit the distribution of Cu and Pt, suggesting an alloying structure of PtCu NSs. All these experimental data from XRD, TEM and XPS prove the successful synthesis of PtCu NSs.

3.2. Hydrogen evolution reaction of PtCu NSs

The electrocatalytic activity of PtCu NSs/C, Pt/C and PtCu NPs/C catalysts toward HER in 0.5 M H_2SO_4 solutions was investigated. As presented in Fig. 3A, PtCu NSs/C shows excellent HER activity with an ultralow onset potential at 2 mA/cm^2 as low as 18 mV (vs. RHE). At a current density of 10 mA/cm^2, its overpotential is only 26.8 mV, while they are as high as 32.0 mV and 35.8 mV for PtCu NPs/C and commercial Pt/C, respectively, demonstrating that PtCu NSs/C has outstanding HER electrocatalytic properties, which is also superior to most Pt based catalysts recently reported (Table S2). As displayed in Fig. S7, PtCu NSs/C presents a higher double-layer capacitance (Cdl ∼ 11.7 mF cm^2) than PtCu NPs/C (Cdl ∼ 10.4 mF cm^2) and Pt/C (Cdl ∼ 9.8 mF cm^2), indicating large intrinsic electrochemical active surface area.

As displayed in Fig. 3B, the Tafel slope of PtCu NSs/C (28.4 mV/dec) is lower than that of Pt/C (32.1 mV/dec) and PtCu NPs/C (30.1 mV/dec). Furthermore, as shown in Fig. 3C, normalized to the Pt loading, at an overpotential of 0.03 V, the HER mass activity of PtCu NSs/C is 1.08 A/mg$_{Pt}$, which is 7.2 and 4 times higher than that of PtCu NPs/C (0.27 A/mg$_{Pt}$) and Pt/C (0.15 A/mg$_{Pt}$), respectively.

The HER stability of PtCu NSs/C, Pt/C and PtCu NPs/C was also investigated. For PtCu NPs/C, after continuous CV cycles for 5000 cycles in 0.5 M H_2SO_4 at a sweep rate of 100 mV/s between −0.1 V and 0.2 V, it presents an almost unchanged behavior (Fig. 3D). The time-dependent overpotential curve of PtCu NSs/C at a static current density of 10 mA/cm^2 for 10 h (Inset diagram in Fig. 3D,) also confirms its excellent stability with the long-term HER electrochemical processes. On the contrary, for PtCu NPs/C and Pt/C, the potential cycling causes an obvious negative
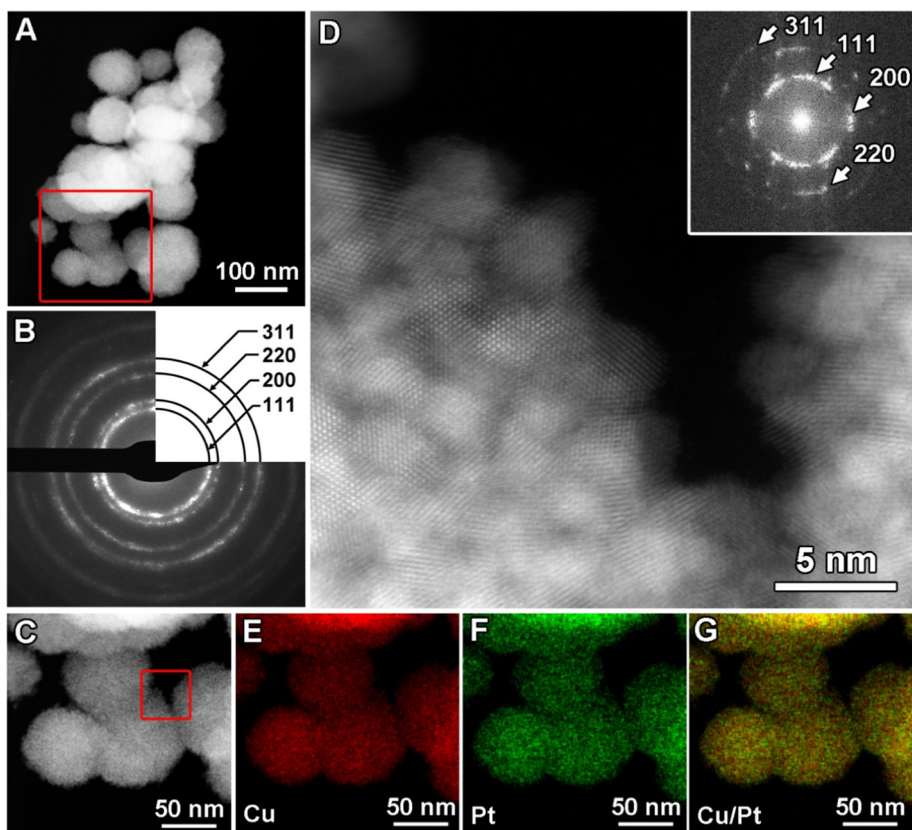
Fig. 2. (A) Low magnification HAADF-STEM image. (B) SAED pattern of the whole area in (A). (C) high magnification HAADF-STEM image of the area indicated by the red box in (A). (D) high resolution HAADF-STEM image of the area indicated by red box in (C) and corresponding FFT pattern of the whole area (inset). (E-G) corresponding EDX elemental maps of the whole area in (D): Cu (red) and Pt (green).
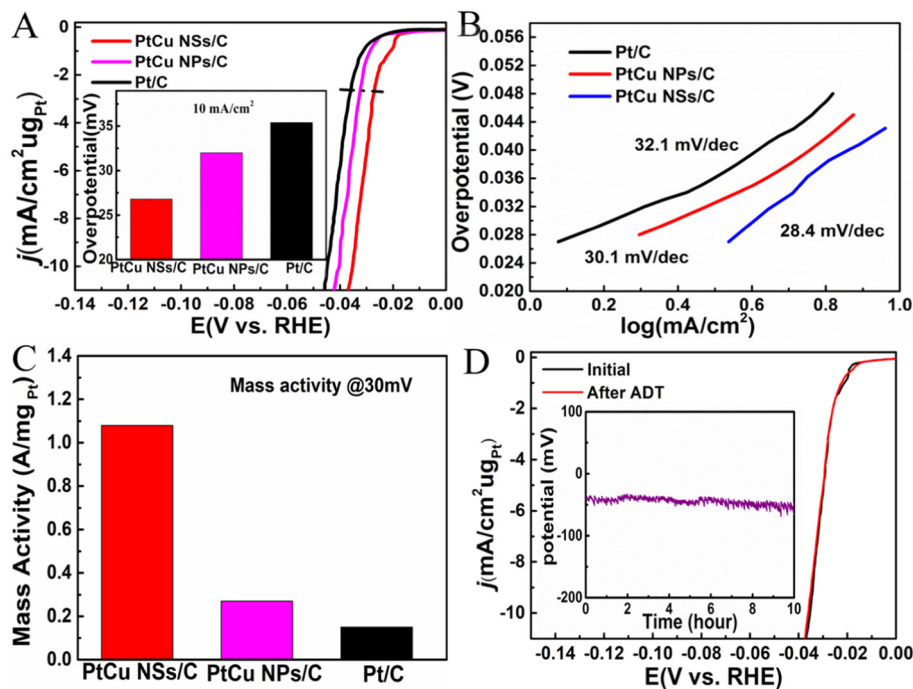

Fig. 3. HER performances of Pt/C, PtCu NPs/C and PtCu NSs/C catalysts in 0.5 M H_2SO_4. (A) HER LSV curves of Pt/C, PtCu NPs/C and PtCu NSs/C (Normalized to Pt loading). The insert diagram is the overpotential of the catalysts. (B) Corresponding Tafel curves obtained from the polarization lines in figure A. (C) Mass activity of Pt/C, PtCu NPs/C and PtCu NSs/C (Normalized to Pt loading). (D) LSV polarization curves of PtCu NSs/C before and after 5000 cycles (Normalized to Pt loading); the insert diagram is time-dependent overpotential curve of PtCu NSs/C at a static current density of 10 mA cm^{-2} for 10 h.

shift of the potential (3 mV) and (13.1 mV) at 10 mA/cm^2 (Fig. S8 and S9). The lower stability of the Pt/C catalysts is due to the weak interaction between the supported Pt particles and the carbon substrate, resulting in a detachment and/or agglomeration of Pt NPs [32,33].

3.3. Oxygen reduction reaction of PtCu NSs

The ORR performance of the catalysts was evaluated in a 0.1 M HClO$_4$ solution. As exhibited in Fig. 4A, by calculating the charge formed during the hydrogen adsorption/desorption processes, PtCu NSs/C and PtCu NPs/C catalysts possess electrochemically active surface area (ECSA) of 73.9 and 65.9 m^2/g$_{Pt}$, respectively, higher than that of commercial Pt/C (62.4 m^2/g$_{Pt}$).

Fig. 4B shows the ORR polarization curves of the catalysts in an O$_2$-saturated 0.1 M HClO$_4$ solution at a sweep rate of 10 mV/s and a rotation rate of 1600 rpm. The PtCu NSs/C catalyst displays an ORR onset potential of 0.978 V, higher than that of Pt/C (0.968 V). The half-wave potential ($\Delta E_{1/2}$) of PtCu NSs/C and PtCu NPs/C is 0.893 V and 0.881 V (vs. RHE), respectively, corresponding to 30 mV and 18 mV positive shifts compared with that of commercial Pt/C (0.863 V). To evaluate the intrinsic ORR activity of the catalysts, their mass activity and specific activity at 0.9 V (vs. RHE) were compared. PtCu NSs/C presents a remarkably high mass activity of 0.42 A/mg$_{Pt}$ at 0.9 V, about 3.2 and 2.1 times higher than that of Pt/C (0.13 A/mg$_{Pt}$) and PtCu NPs/C (0.20 A/mg$_{Pt}$), respectively. In addition, PtCu NSs/C also exhibits an outstanding specific activity (0.57 mA/cm^2), which is 2.7 times and 1.8 times higher than that of Pt/C (0.21 mA/cm^2) and PtCu NPs/C (0.31 mA/cm^2). Table S3 lists the ORR activity parameters of Pt based ORR catalysts in acidic media. Interestingly, the 3D PtCu NSs developed in this study exhibit favorably high activity compared with the most PtCu catalysts as reported recently. As presented in Fig. S7, the Tafel slope (79.2 mV/dec) of PtCu NSs/C is lower than that of Pt/C (83.3 mV/dec) and PtCu NPs/C (88.6 mV/dec), suggesting much faster electron transfer rate and superior ORR activity compared to Pt/C.

The stability of the catalysts was explored by accelerated degradation tests (ADT). The ORR polarization curves for PtCu NSs/C and Pt/C catalysts are shown in Fig. 4C. After 10,000 potential cycles, only a small decline of $\Delta E_{1/2}$ can be observed for PtCu NSs/C, compared with 27 mV for commercial Pt/C. The mass activity calculated from the ORR polarization curves before and after ADT is also used to characterize the stability of the electrocatalytic activity: the mass activity of Pt/C and PtCu NSs/C catalysts decreases to 0.07 and 0.37 A/mg$_{Pt}$, corresponding to about 48% and 13% of their original values (Fig. 4D), respectively. Based on the above results, it is clearly shown that the PtCu NSs/C catalyst possesses greatly improved durability.

This remarkable enhancement in ORR activity for PtCu NSs can be attributed to the following reasons: (1) Due to the Pt-rich outer surface structure, more active sites of Pt exposed in the sphere structure facilitate the dissociation of O$_2$, thus leading to dramatically enhanced ORR performance with an increased utilization of Pt; (2) More Cu is introduced into PtCu NSs, promoting a lattice contraction and a downshift of the d-band [34]; (3) Compared to 0D nanoparticle, the PtCu NSs in this work are composed of nanoparticles connected each other with a large number of voids inside, providing more catalytic active sites and mass transfer passages [7,35].

The morphology and composition of PtCu NSs were characterized after ADT test. As shown in Fig. S11A–D, the NSs still contain Pt and Cu elements. The line-profile analysis using STEM-EDS along one PtCu NS (Fig. S11E) further confirms that Cu is concentrated in the core region with a Pt-rich surface.

As to the origin of the dramatically enhanced lifetime, at least three main aspects are proposed: (1) the Pt located in surface layer of the PtCu alloy has a very solid structure, as a result of the surface compressive strain; (2) At the same time, the Cu dissolution from the subsurface regions of the nanospheres is considerably blocked owing to formation of the Pt surface layer for the PtCu alloy
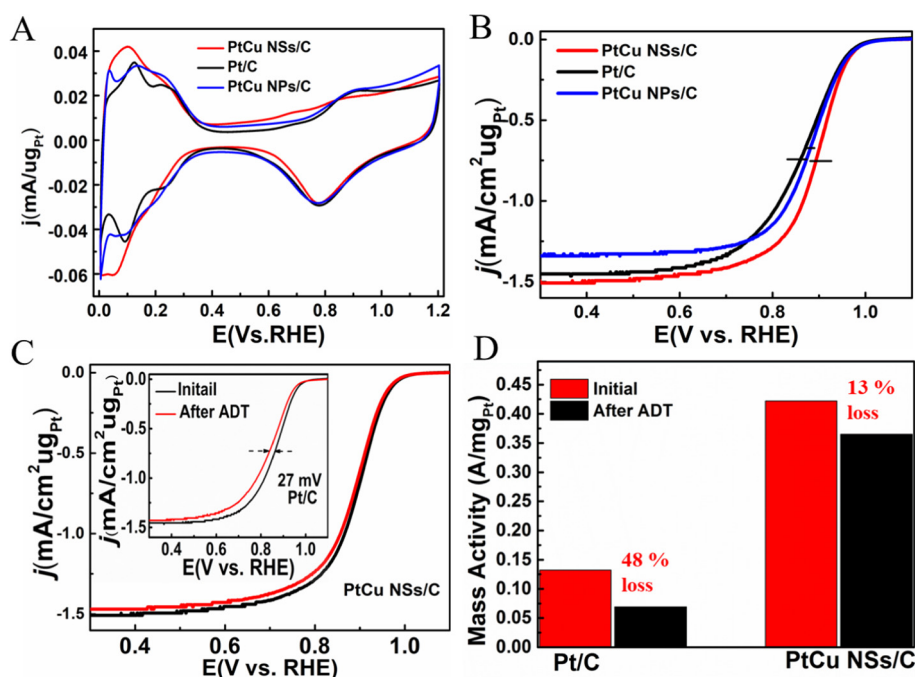

Fig. 4. (A) Cyclic voltammetry curves of PtCu NSs/C, PtCu NPs/C and Pt/C catalysts in N$_2$-saturated 0.1 M HClO$_4$ solutions with a sweep rate of 50 mV/s. (B) ORR LSVs of PtCu NSs/C, PtCu NPs/C and Pt/C catalysts in O$_2$-saturated 0.1 M HClO$_4$ solutions at sweep rate of 10 mV/s and rotation rate of 1600 rpm. (C) ORR polarization curves of PtCu NSs/C and commercial Pt/C (inset) before and after 10,000 cycles. (D) Mass activity of Pt/C and PtCu NSs/C catalysts before and after 10,000 cycles for ORR at 0.9 V vs. RHE. All are normalized to Pt loading.
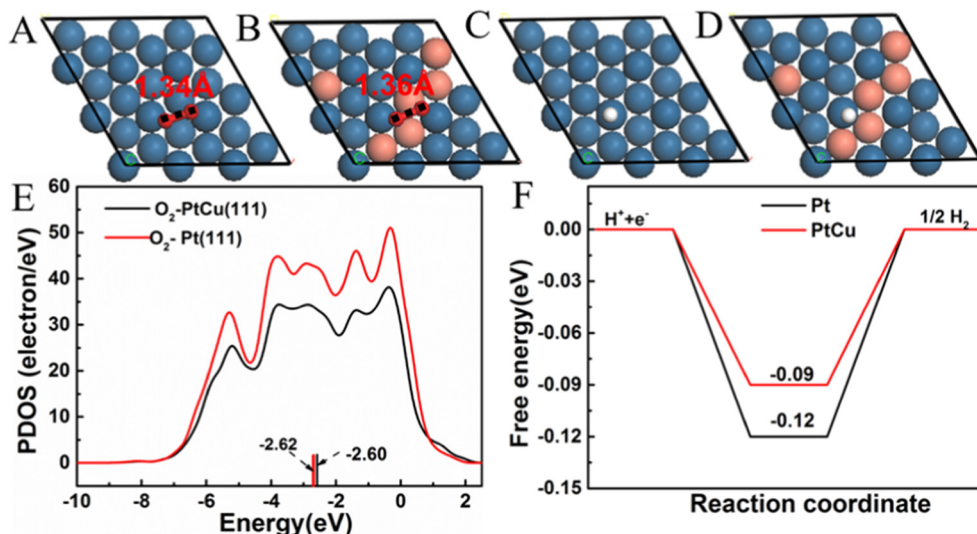
Fig. 5. Model of oxygen adsorbed on Pt (1 1 1) (A) and PtCu (1 1 1) (B). (C-D) The possible hydrogen adsorbed structures on the Pt (1 1 1) and (B) PtCu (1 1 1) (E) PDOS of d orbitals of Pt (1 1 1) and PtCu (1 1 1). The calculated d-band centers are marked with lines. (F) Free energy diagram for hydrogen evolution at Pt(1 1 1) and PtCu(1 1 1).

[36,37]; (3) Due to the rough sphere structure, the interaction between NSs and carbon supports is stronger than that of Pt/C, rendering a much high stability [38,39].

3.4. Mechanism analysis toward the high catalytic performance of PtCu NSs

DFT calculations were carried out to forecast the catalytic activity for Pt-Cu catalysis. The enhanced O_2 adsorption energy and the weakened O—O bond result in a fast scission of the O—O bond, subsequently enhancing the O_2 reduction performance [31,36]. The high O_2 adsorption energy indicates that the O_2 coverage on the surface of catalyst is enhanced [40]. According to the model presented in Fig. 5A,B, the O_2 adsorption energy (ΔE_{O2}) and the O—O bond on Pt-Cu (1 1 1) slabs are 1.37 eV and 1.36 Å, respectively, larger than that of Pt (1 1 1) slabs (1.36 eV, 1.34 Å). Therefore Pt alloying with Cu can facilitate the ORR performance.

The d-band center is another important parameter for evaluating the ORR performance. The down-shifted d-band center of Pt makes the adsorption energies of surface species (such as OH_{ads}) decrease, resulting in a lower coverage of such species on catalyst surfaces and more available active sites for oxygen dissociation which increases the ORR activity of Pt [41–44]. As shown in Fig. 5E, the d-band center of pure Pt (−2.60 eV) downshifts to −2.62 eV after alloying with Cu.

It is well known that an active HER catalyst would necessarily have the free energy of hydrogen adsorption GH* as close to 0 as possible [45]. After calculating GH* on Pt (1 1 1) and PtCu (1 1 1) planes (Fig. 5C,D), we found that the GH* on a PtCu (1 1 1) surface (−0.09 V) is much smaller than that on Pt (1 1 1) (−0.12 V), even closer to 0 than that of Pt(1 1 1) (Fig. 5F). This suggests that the adsorbed hydrogen energy of PtCu is neither too weak nor too strong, making it possible possess a high activity for HER [46].

4. Conclusion

3D PtCu nanospheres (NSs) consisting of nano-single crystal particles were successfully synthesized by a simple, cost-effective, aqueous solution method. The obtained PtCu NSs with a Pt-rich surface structure, exhibited a greatly catalytic activity and durability toward both HER and ORR in acidic media compared to the commercial Pt/C catalyst (7.2-folds improvement in mass

activity at 30 mV for HER, and 3.2-folds enhancement in mass activity at 0.9 V for ORR). The unique 3D structure and the alloying effect account for the significant improvement of the electrocatalytic performance of the PtCu NSs. Our work provides a promising approach to designing highly active and stable next-generation catalysts with a substantial reduction in Pt amount.

Appendix A. Supplementary material

Supplementary data to this article can be found online at https://doi.org/10.1016/j.jcat.2019.05.031.

References

[1] M. Winter, R.J. Brodd, Chem. Rev. 104 (2004) 4245–4269.
[2] Y. Liang, Y. Li, H. Wang, J. Zhou, J. Wang, T. Regier, H. Dai, Nat. Mater. 10 (2011) 780–786.
[3] C. Chen, Y. Kang, Z. Huo, Z. Zhu, W. Huang, H.L. Xin, J.D. Snyder, D. Li, J.A. Herron, M. Mavrikakis, Science 343 (2014) 1339–1343.
[4] J. Xie, J. Zhang, S. Li, F. Grote, Z. X, H. Zhang, R. Wang, Y. Lei, P. B, Y. Xie, J. Am. Chem. Soc. 135 (2013) 17881–17888.
[5] J.Y. Park, D.H. Kwak, K.B. Ma, S.B. Han, G.S. Chai, S.K. Kim, D.H. Peck, C.S. Kim, A. Kucernak, K.W. Park, J. Catal. 359 (2018) 46–54.
[6] M.K. Debe, Nature 486 (2012) 43–51.
[7] H.Y. Kim, S. Cho, Y.J. Sa, S.M. Hwang, G.G. Park, T.J. Shin, H.Y. Jeong, S.D. Yim, S. H. Joo, Small 12 (2016) 5347–5353.
[8] D. He, L. Zhang, D. He, G. Zhou, Y. Lin, Z. Deng, X. Hong, Y. Wu, C. Chen, Y. Li, Nat. Commun. 7 (2016) 12362.
[9] S.Y. Huang, P. Ganesan, B.N. Popov, Acs Catal. 2 (2012) 825–831.
[10] S.J. Hwang, S.K. Kim, J.G. Lee, S.C. Lee, J.H. Jang, P. Kim, T.H. Lim, Y.E. Sung, S.J. Yoo, J. Am. Chem. Soc. 134 (2012) 19508–19511.
[11] L. Hou, H. Qiu, J. Power Sour. 216 (2012) 28–32.
[12] H. Wang, S. Xu, C. Tsai, Y. Li, C. Liu, J. Zhao, Y. Liu, H. Yuan, F. Abild-Pedersen, F. B. Prinz, J.K. Nørskov, Y. Cui, Science 354 (2016) 1031.
[13] X. Zhang, H. Wang, J. Key, V. Linkov, S. Ji, X. Wang, Z. Lei, R. Wang, J. Electrochem. Soc. 159 (2012) B270–B276.

[14] L. Bu, S. Guo, X. Zhang, X. Shen, D. Su, G. Lu, X. Zhu, J. Yao, J. Guo, X. Huang, Nat. Commun. 7 (2016) 11850.
[15] V.R. Stamenkovic, B. Fowler, B.S. Mun, G. Wang, P.N. Ross, C.A. Lucas, N.M. Marković, Science 315 (2007) 493–497.
[16] Y. Xiong, L. Xiao, Y. Yang, F.J. DiSalvo, H.D. Abruña, Chem. Mater. 30 (2018) 1532–1539.
[17] X.L. Lei, M.S. Wu, G. Liu, B. Xu, C.Y. Ouyang, J. Phys. Chem. A 117 (2013) 8293–8297.
[18] X. Du, S. Luo, H. Du, M. Tang, X. Huang, P.K. Shen, J. Mater. Chem. A 4 (2016) 1579–1585.
[19] S. Nardecchia, D. Carriazo, M.L. Ferrer, M.C. Gutierrez, F.D. Monte, Chem. Soc. Rev. 42 (2013) 794–830.
[20] C. Wang, H. Daimon, T. Onodera, T. Koda, S. Sun, Angew. Chem. 47 (2008) 3588.
[21] C. Wang, H. Daimon, Y. Lee, J. Kim, S. Sun, J. Am. Chem. Soc. 129 (2007) 6974–6975.
[22] S. Sun, G. Zhang, Y. Zhong, H. Liu, R. Li, X. Zhou, X. Sun, Chem. Commun. 18 (2009) 7048–7050.
[23] Z. Chen, M. Waje, W. Li, Y. Yan, Angew. Chem. Int. Ed. 46 (2007) 4060.
[24] S. Sun, G. Zhang, D. Geng, Y. Chen, R. Li, M. Cai, X. Sun, Angew. Chem. 123 (2011) 442–446.
[25] X. Huang, Z. Zhao, L. Cao, Science 348 (2015) 1230–1234.
[26] E.A. Anumol, A. Halder, C. Nethravathi, B. Viswanatha, N. Ravishankar, J. Mater. Chem. 21 (2011) 8721–8726.
[27] L. Xiong, A.M. Kannan, A. Manthiram, Electrochem. Commun. 4 (2002) 898–903.
[28] W. Li, I.S. Amiinu, B. Wei, W. Zhe, J. Zhu, Z. Kou, S. Mu, ChemSusChem 11 (2018) 1328–1333.
[29] C.Y. He, S.K. Zhang, J.Z. Tao, P.K. Shen, J. Catal. 362 (2018) 85–93.
[30] H. Duan, Q. Hao, C. Xu, J. Power Sour. 280 (2015) 483–490.
[31] Y. Wang, K. Yin, J. Zhang, C. Si, X. Chen, L. Lv, W. Ma, H. Gao, Z. Zhang, J. Mater. Chem. A 4 (2016) 14657–14668.
[32] Y. Liu, W.E. Mustain, Int. J. Hydrogen Energ. 37 (2012) 8929–8938.
[33] N. Cheng, S. Stambula, W. Da, M.N. Banis, L. Jian, A. Riese, B. Xiao, R. Li, T.K. Sham, L.M. Liu, Nat. Commun. 7 (2016) 13638.
[34] Y. Zhao, Y. Wu, J. Liu, F. Wang, Acs Appl. Mater. Interf. 9 (2017) 35740–35748.
[35] D. Shen, L. Chen, J. Yang, R. Zhang, Y. Wei, X. Li, W. Li, Z. Sun, H. Zhu, A.M. Abdullah, A. Al-Enizi, A.A. Elzatahry, F. Zhang, D. Zhao, ACS. Appl. Mater. Interf. 31 (2015) 17450–17459.
[36] J. Liu, M. Jiao, L. Lu, H.M. Barkholtz, Y. Li, Y. Wang, L. Jiang, Z. Wu, D.J. Liu, L. Zhuang, C. Ma, J. Zeng, B. Zhang, D. Su, P. Song, W. Xing, W. Xu, Y. Wang, Z. Jiang, G. Sun, Nat. Commun. 8 (2017) 15938.
[37] C. Wang, M. Chi, D. Li, D. Strmcnik, D.V.D. Van, G. Wang, V. Komanicky, K.C. Chang, A.P. Paulikas, D. Tripkovic, J. Am. Chem. Soc 133 (2011) 14396–14403.
[38] B.Y. Xia, W.T. Ng, H.B. Wu, X. Wang, X.W. Lou, Angew. Chem. 124 (2012) 7325–7328.
[39] S. Guo, D. Li, H. Zhu, S. Zhang, N.M. Markovic, V.R. Stamenkovic, S. Sun, Angew. Chem. 125 (2013) 3549–3552.
[40] T. Toda, H. Igarashi, M. Watanabe, J. Electroanal. Chem. 460 (1999) 258–262.
[41] Y.C. Tseng, H.S. Chen, C.W. Liu, T.H. Yeh, K.W. Wang, J. Mater. Chem. A 2 (2014) 4270–4275.
[42] N. Jung, Y. Sohn, H.P. Jin, K.S. Nahm, P. Kim, S.J. Yoo, Appl. Catal. B Environ. 196 (2016) 199–206.
[43] J.K. Nørskov, T. Bligaard, A. Logadottir, S. Bahn, L.B. Hansen, M. Bollinger, H. Bengaard, B. Hammer, Z. Sljivancanin, M. Mavrikakis, J. Catal. 209 (2002) 275–278.
[44] V. Stamenkovic, B.S. Mun, K.J. Mayrhofer, P.N. Ross, N.M. Markovic, J. Rossmeisl, J. Greeley, J.K. Nørskov, Angew. Chem. 118 (2006) 2963–2967.
[45] J.K. Noerskov, T. Bligaard, A. Logadottir, J.R. Kitchin, J.G. Chen, S. Pandelov, U. Stimming, J Electrochem. Soc. 152 (2005) J23–J26.
[46] T. Chao, X. Luo, W. Chen, B. Jiang, J. Ge, Y. Lin, G. Wu, X. Wang, Y. Hu, Z. Zhuang, Y. Wu, X. Hong, Y. Li, Angew. Chem. Int. Ed. Engl. 129 (2017) 16263–16267.